PERGAMON

Vision Research 38 (1998) 1731–1743

Vision Research

Large receptive fields for optic flow detection in humans

David C. Burr [a,b,*], M. Concetta Morrone [a], Lucia M. Vaina [c]

[a] *Istituto di Neurofisiologia del CNR, Via S. Zeno 51, Pisa 56217, Italy*
[b] *Dipartimento di Psicologia, Università di Firenze, Florence, Italy*
[c] *Department of Biomedical Engineering, College of Engineering, Boston University, Boston, MA, USA*

Received 10 June 1997; received in revised form 19 September 1997

Abstract

We used a psychophysical summation technique to study the properties of detectors tuned to radial, circular and translational motion, and to determine the spatial extent of their receptive fields. Signal-to-noise motion thresholds were measured for patterns curtailed spatially in various ways. Sensitivity for radial, circular and translational motion increased with stimulus area at a rate predicted by an ideal integrator. When sectors of noise were added to the stimulus, sensitivity decreased at a rate consistent with an ideal integrator. Summation was tested for large annular stimuli, and shown to hold up to 70° in some cases, suggesting very large receptive fields for this type of motion (consistent with the physiology of neurones in the dorsal region of the medial superior temporal area (MSTd)). This is a far greater area than observed for summation of contrast sensitivity to gratings (Anderson SJ and Burr DC, Vis Res 1987;29:621–635, and to this type of stimuli (Morrone MC, Burr DC and Vaina LM, Nature 1995;376:507–509, consistent with the suggestion that the two techniques examine different levels of motion analysis.

Keywords: Motion; Optic flow; Summation; Receptive fields; Heading

1. Introduction

Movement through the environment produces deformations of the optic array, commonly referred to as the optic flow field [3]. The computation of optic flow is fundamental for orientation and visual navigation in three-dimensional space, for the perception of object movement, for stabilising the visual world and for the control of posture and locomotion. Optic flow on the retina can be decomposed into elementary components independent of the co-ordinate system chosen: div (radial motion), curl (circular motion), translation and possibly deformation [4–7].

In the dorsal region of the medial superior temporal area (MSTd) of monkey cerebral cortex, neurones have been shown to respond to the components of optic flow: translational, radial and circular motion ([8–19]; see [20] for review). These neurones, as well as other parietal neurones tuned to radial motion, respond best to large stimuli, indicating extensive spatial summation [10,12,14,21]. The optic-flow sensitive neurones have large receptive fields (10–100° diameter) many of which extend over both contralateral and ipsilateral visual hemifields, with no strong correlation between receptive field size and the retinal eccentricity of the centre of the receptive field. The response of these neurones is insensitive to dot density, to image speed and often also to stimulus position [14,15]. It also does not distinguish local object motion from global field motion, even when clear boundary information is available [22]. Taken together, these properties make MSTd neurones likely candidates for the computation of optic flow information. They are clearly more suitable than the directionally tuned neurones earlier in the motion hierarchy, such as V1 or MT, whose receptive fields subtend only a limited fraction of the optic flow stimulation.

Most models for MST motion selectivity assume input from a range of MT cells (consistent with the known anatomy: [23,24]). Tanaka and Saito [12] proposed that each MSTd cell that is responsive to a particular complex motion trajectories integrates inputs from an array of MT cells of appropriate directional

* Corresponding author. Tel.: +39 50 559719; fax: +39 50 559725; e-mail: dave@neuro.in.pi.cnr.it.

0042-6989/98/$19.00
PII: S0042-6989(97)00346-5

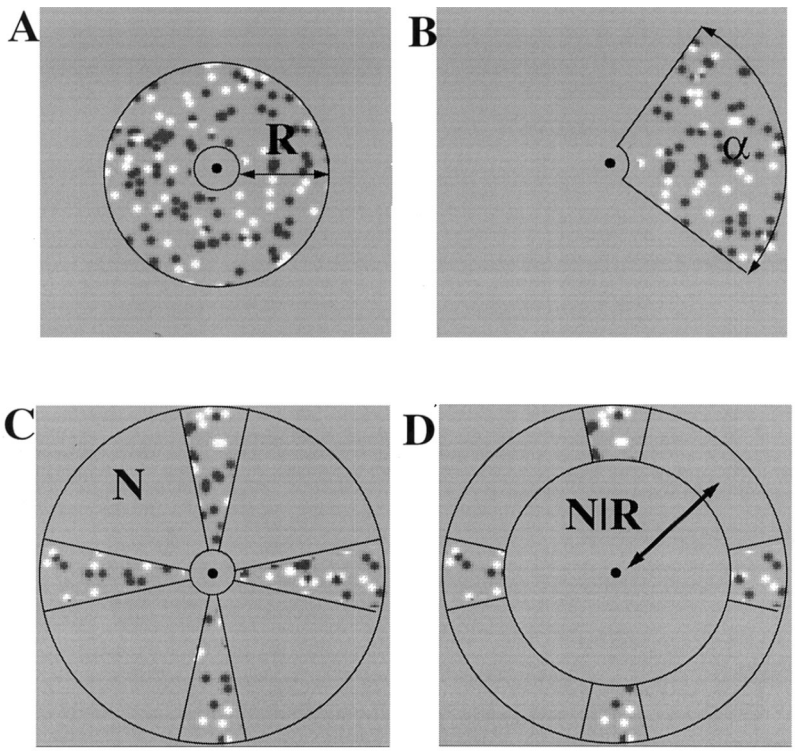

Fig. 1. Examples of the curtailed stimuli used for this study. (A) Concentric circles of variable radius R (ommiting the central region of radius 10 pixels). (B) A single sector subtending α clock°. (C) Several sectors, each subtending 22.5 clock°. (D) An annulus (with the central circle of radius 45 pixels) was removed. This was further divided into several sectors, each subtending 22.5 clock°, having a near square aspect ratio.

tuning distribution of receptive fields. For example, radial cells integrate inputs from MT cells whose receptive fields positions and preferred directions are arranged radially. To account for positional invariance of directional selectivity within the receptive field of MSTd cells they suggested that the receptive fields of MSTd cells comprise several compartments, each performing integration within its own small territory, independently from the others [8]. Although such a mechanism has certain advantages, it does not account for all the more recent findings, such as the demonstration of Duffy and Wurtz [14] and Graziano et al. [13] that MSTd neurones often respond not only to one component (such as pure radial motion), but to two or three components of motion (such as spiral motion, the combination of radial and circular motion).

The sensitivity of the human visual system to optic flow stimuli has been studied by psychophysical means. The first evidence for detectors specialised for radial motion, or 'looming detectors', was provided by Regan and Beverley [25,26]. In a series of adaptation experiments, they showed that adaptation to expanding and contracting stimuli decreases sensitivity to these motions in a way that cannot be accounted for by the local motion of the elements of expansion. The same was also true when stimuli were caused to move in a circular motion [27]. These results suggest the existence of mechanisms selectively sensitive to radial or circular motion distinct from the basic motion mechanisms that signal change in speed or linear direction. However, the effects of Regan and Beverley held only for stimuli subtending less than 1° [28], suggesting very small receptive fields for the looming detectors, not consistent with the more recent electrophysiology of MSTd neurones discussed above.

Other evidence suggesting the existence of specialised mechanisms for complex motion has been provided by a series of masking studies and adaptation studies [29–32]. Freeman and Harris [30] reported that sensitivity (defined as the slowest detectable speed of motion in random dot patterns) is significantly greater for radial and circular patterns than for translational patterns or incoherently moving dots with identical distribution of local motion. A possible explanation of this result is a linear pooling of local motion by specialised mechanisms for radial and circular motion. This idea is reinforced by a recent study of Bex and Makous [33], showing that radial motion appears faster than translational motion of the same physical speed.

The physiology suggests that the mechanisms that respond specifically to complex motion are situated in an area assumed to be involved at a relatively high level

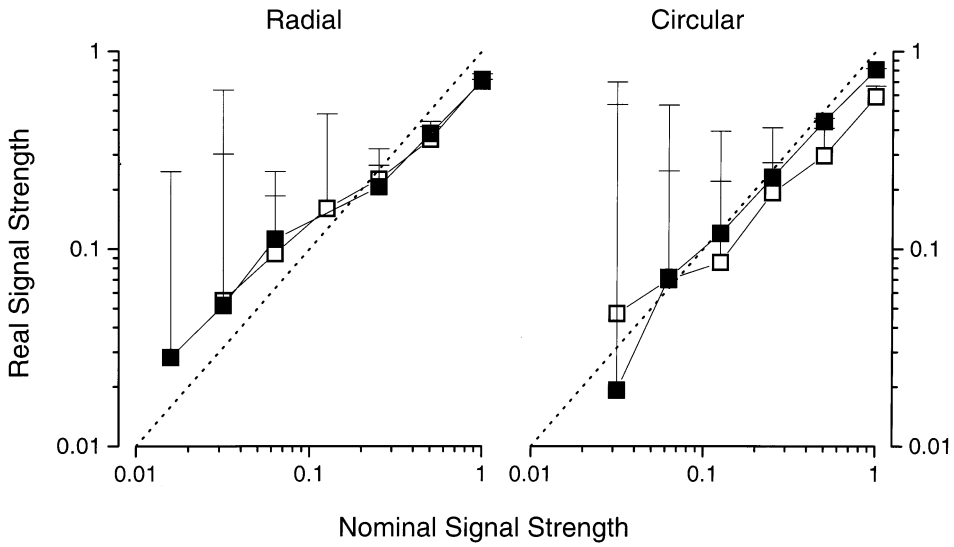

Fig. 2. Monte Carlo simulations of the strength of the motion signal, as a function of proportion of coherently moving dots. Signal strength was calculated as the integral of the product of the third frame moved back along the inverted direction of motion and the second undisplaced frame divided by average overall power of the two frames. Each point is the average of 20 simulations with fresh random draws, and the error bars show +1 S.D. There is considerable variability in the real signal strength from one draw to another (indicated by error bars), particularly at low signal levels, and there were also systematic errors (deviations from the dotted line). This variation was compensated for by calculating the stimuli prior to the experiment, and assigning them to the appropriate S/N bin. Filled symbols refer to 16-sector stimuli, and open symbols to one-sector stimuli.

of analysis (MST). It is not clear that the psychophysical techniques discussed above will necessarily probe this site. Adaptation and masking may well influence the response of MST neurones, but they may also influence the response of neurones at earlier sites such as V1 or MT, complicating the interpretation of results.

In a recent study Morrone et al. [2] applied a summation technique to study mechanisms tuned to optic flow fields. Signal-to-noise sensitivity increased in a predictable way with the area of a spatially curtailed circle, for radial, circular and translational motion, implying that motion of opposing directions is integrated by specialised neural mechanisms (see Fig. 3 for more details). However, contrast sensitivity did not increase with stimulus area, except over a very small range (about 1°). This is consistent with contrast sensitivity being limited at an early level (such as V1) that may impose a contrast threshold. Further experiments showed that summation for contrast sensitivity did occur when the stimuli were particularly noisy, forcing the limit of sensitivity to be set by a later stage. The results fit well with the electrophysiological evidence for detectors of complex motion in MSTd, after contrast thresholding in V1.

In this study we extend the technique of the preliminary study to explore further the spatial properties of detectors tuned to optic flow patterns, and to investigate the extent of the summation. The results show that summation can occur over very large areas, consistent with the existence of optic-flow detectors with very large receptive fields, as the physiological evidence would suggest.

2. Methods

2.1. Stimuli

The stimuli were four-frame random-dot cinematograms, falling within a 128×128 pixel square,

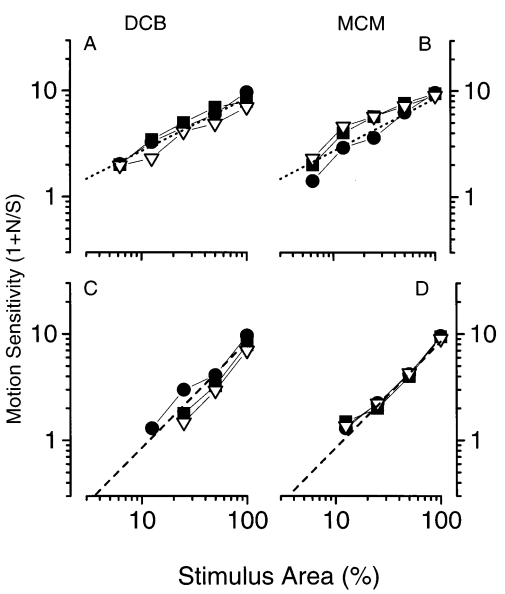

Fig. 3. Motion sensitivity for correctly discriminating the direction of radial, circular and translational motion as a function of stimulus area (reproduced with permission from Ref. [2]). In the upper curves (figures C and D) they were filled with noise dots of the same average density as the other sectors. The dotted lines indicate a square-root relationship between sensitivity and area and the dashed lines a linear relationship. Both predictions are quite good. The best fitting slopes, or summation indexes, are given in Table 1.

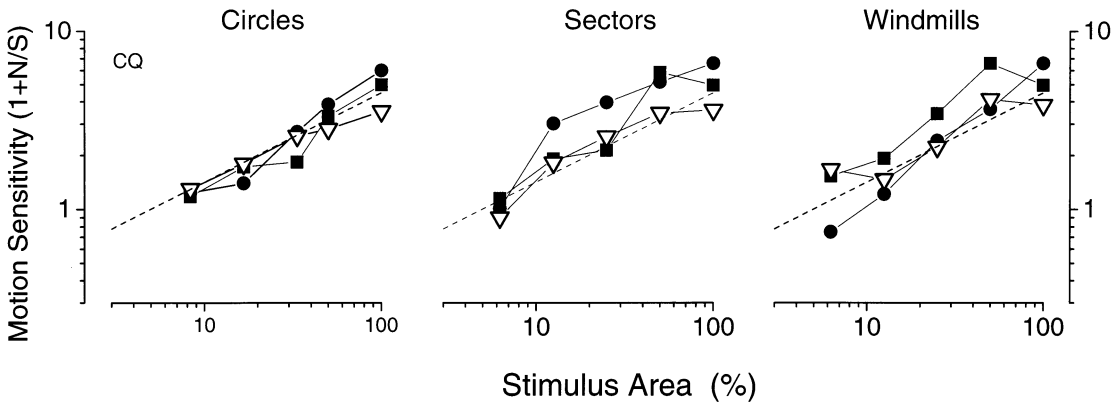

Fig. 4. Motion sensitivity of radial (square symbols), circular (circles) and translational (triangles) motion as a function of stimulus area, for three different type of curtailment: Left, reducing the radius of the circle; Centre, reducing the circle to a single sector of variable angle; Right, dividing the circle into several oppositely positioned sectors, each subtending 22.5 clock degress. The dashed line has slope of 0.5, indicating a square-root relationship between sensitivity and area. The summation indexes for the nine conditions are given in Table 1.

comprising 360 black or white Gaussian patches (space constant ± 1 pixel) caused to move coherently along radial, circular or translational trajectories. The four frames were faded in and out at a variable rate through a symmetrical envelope, with the first and last frames attenuated by a factor of 18. The impression of motion was generated by displacing dots by 4 pixels on each frame (lifetime two frames) in appropriate directions: horizontally (left or right), radially or along circular trajectories. As the displacement size was always 4 pixels, irrespective of distance from centre, the circular motion did not correspond exactly to rotation of a rigid body, nor radial motion to real expansion or contraction. However, this procedure allowed dot density to remain constant, as well as facilitating comparison between the three types of motion.

To study summation the area of the stimuli was curtailed in various ways, some of which are illustrated in Fig. 1. The diameter could be reduced (Fig. 1(A)), the circle could be gated to a single sector of varying angle (Fig. 1(B)) or a variable number of oppositely positioned sectors, each subtending 22.5 clock° (Fig. 1(C)). In all cases, a small central region of radius 10 pixels was left blank. For the experiments probing receptive field size, the stimuli were based on an annulus rather than a circle, to stimulate the peripheral visual field. This stimulus could then be curtailed into approximately square segments, as illustrated in Fig. 1(D). For some conditions, the non-signal sectors were not left blank but filled with incoherent noise of the same average density.

Motion sensitivity was determined by measuring the minimum proportion of coherently moving dots that supported reliable direction discrimination (using the

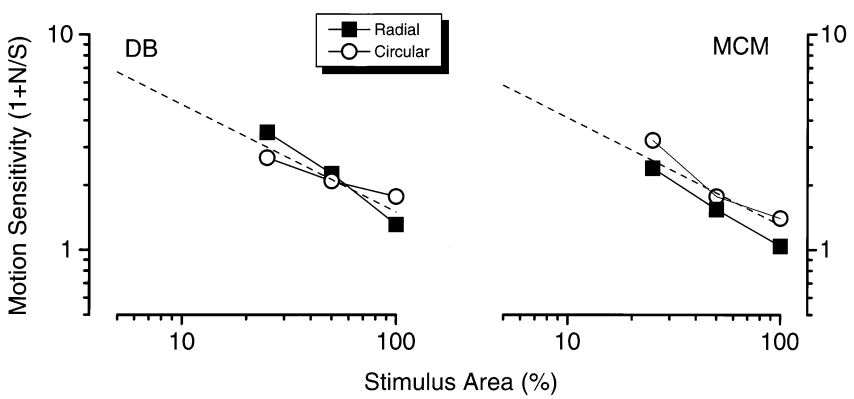

Fig. 5. Effect of filling the non-signal sectors with incoherent noise. Four oppositely positioned sectors contained the motion signal (radial or circular motion). The other 12 sectors were either all blank (corresponding to 25% total noise plus signal stimulus area), included four maximally spaced mask sectors of incoherent noise (50% total area) or were all filled with incoherent noise (100% total area). Motion sensitivity for both radial and circular motion decreased as a function of total stimulus area. The dotted line represents an inverse square-root between sensitivity and image size (slope of -0.5 on log co-ordinates), corresponding to the theoretical predictions of an ideal integrator. The summation indexes are given in Table 1.

adaptive procedure described below). A given proportion of signal dots (chosen at random) moved coherently along a motion trajectory, while the remaining noise dots were plotted to new random positions on each frame. If the movement of a signal dot caused it to exceed the boundaries of the display, or to pass over the confines of the curtailment, it was replaced at a new random position. Nominally, the signal strength should be given by the proportion of signal-to-total dots. However, this may vary randomly from trial to trial because of random correlations in the noise dots, or it may vary more systematically because of the different effects of curtailment of the various types of motion.

To test whether this may be a problem, we calculated the actual motion strength by cross correlation: the integral of the product of the third frame moved back along the inverted direction of motion and the second undisplaced frame was divided by average overall power of the two frames to yield the real signal strength. This was repeated for a series of stimuli with different random draws, at various ratios of signal to total dot number. Fig. 2 illustrates the results for four conditions, expansion and clockwise rotation, each for the full stimuli and for a single 22.5° sector. The error bars (each ± 1 S.D. of 20 runs) show that there is considerable variation in the real signal strength, particularly when the proportion of signal dots is low. Furthermore, there is a systematic underestimation of signal strength in some conditions, particularly the curtailed rotary motion, where the trajectories were short, so the probability of overspilling was high.

To avoid this problem, we prepared the stimuli in advance (on a Silicon Graphics workstation), and calculated the actual signal strength by cross correlation. The stimuli were then classified appropriately (with 0.05 log unit resolution) and stored on disk. For each condition, there were four separate random draws for each signal strength (selected at random during the experiment).

2.2. Psychophysical procedure

The stimuli had 128×128 pixel resolution, pre-prepared on a Silicon Graphics Iris computer, as described above. They were read by a networked PC computer and displayed on a Barco Calibrator Monitor at 170 frames/s, via the Cambridge Research Systems VSG card. The frames in the motion sequence were updated at a variable rate, depending on conditions (specified in figure captions). For the first experiments Figs. 3–5, they occupied an area of 10×10 cm. For the experiments using the annuli stimuli Figs. 6–11, they were expanded to 20×20 cm, by duplicating pixels horizontally and vertically.

For any given session, only one type of motion was displayed (radial, circular etc.), and observers were required to discriminate the direction of each trial (expansion from contraction, clockwise from counterclockwise etc.) by pressing the appropriate button; release of the button initiated the next trail. The files were read while subjects responded to the previous trial, with no noticeable delay. Thresholds were determined by the adaptive QUEST procedure [34] that estimated threshold after each trail, and placed the signal strength of the next near that level (with a random perturbation of ± 0.1 log-units). At least five different QUEST sessions, each of 40 trials, were run for each condition, yielding an estimate of S.E. The final estimate of threshold was calculated by fitting an accumulative Gaussian to the probability of seeing curves.

Viewing distance was varied from condition to condition, reported in each figure caption. All observers had normal or corrected to normal acuity.

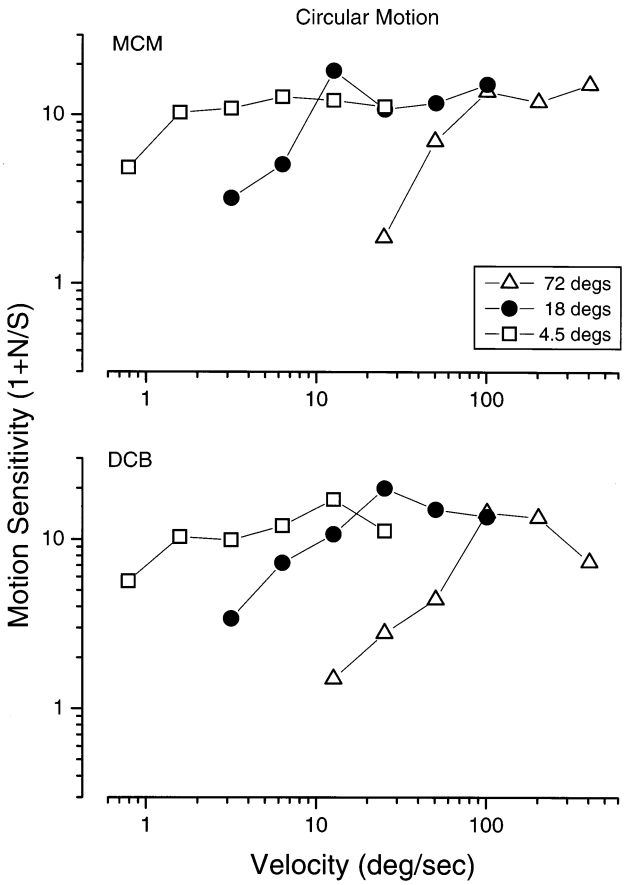

Fig. 6. Motion sensitivity for circular motion within annuli stimuli (inner and outer diameters 14 and 20 cm), as a function of image velocity. The size of the image (outer diameter) was varied from 4.5 to 72° by varying viewing distance from 220 to 14 cm (scaling dot size proportionally). Speed was varied by varying the rate of presentation of the frames, from 170 Hz (the monitor framerate) to 28 Hz (the slowest rate without obvious flicker).

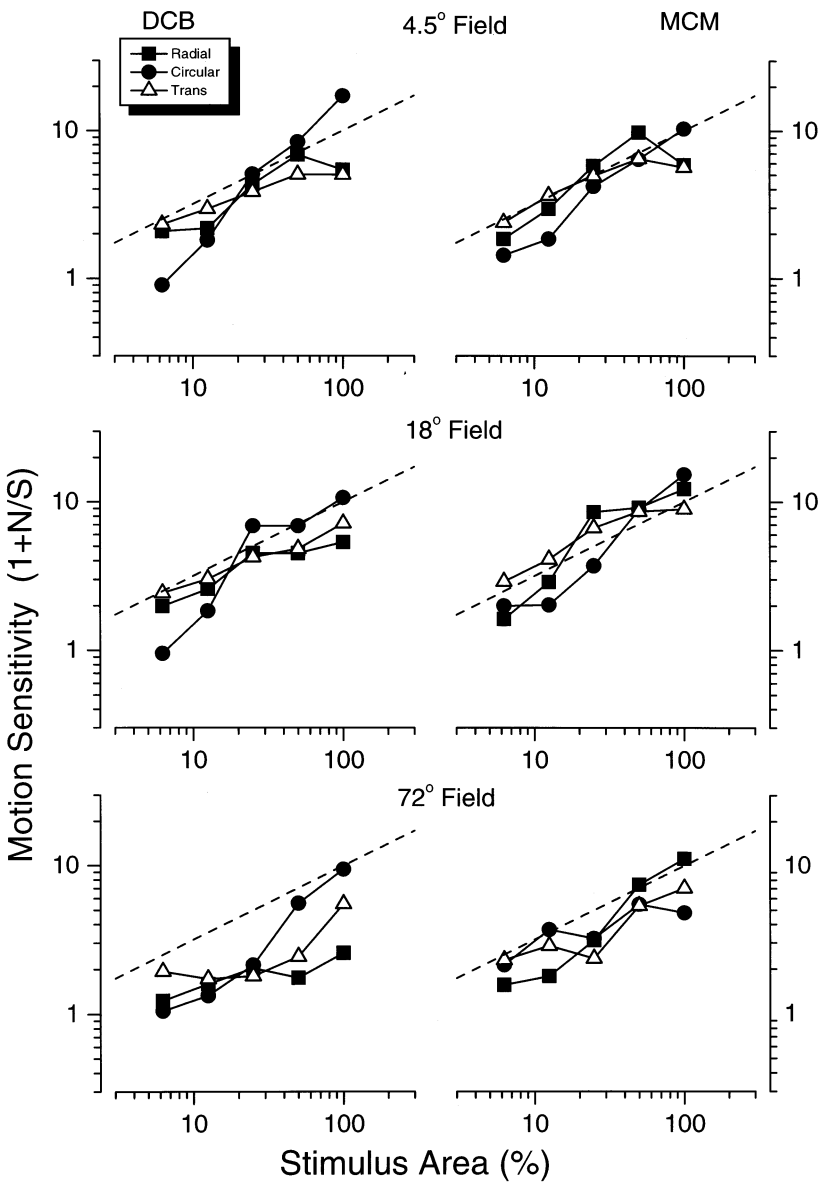

Fig. 7. Motion sensitivity of radial, circular and translational motion of an annulus curtailed into multiple sectors curtailment, for three different annuli sizes (outer diameters). The dotted line represents a square-root relationship between sensitivity and image size, corresponding to the theoretical predictions of an ideal integrator.

3. Results

3.1. Summation of motion signals across complex trajectories

The main technique used throughout this study was to measure how sensitivity varied with stimulus area. Fig. 3 shows results for the basic summation technique, reproduced from Morrone et al. [2]. Motion sensitivity (defined as the minimum proportion of signal to total dots to support reliable direction discrimination) was measured for stimuli curtailed as illustrated in Fig. 1(C), and plotted as a function of stimulus area. In the upper curves the sectors without signal dots were set to mean-luminance. In the lower curves, the non-signal sectors were filled with noise dots of the same density as the other sectors. In both cases sensitivity increased with stimulus area, but the increase was more rapid with noisy non-signal sectors.

The performance of an ideal integrator capable of integrating over the whole display along the given trajectory can be described by d'_e:

$$d'_e = \frac{s}{\sqrt{N_i + N}}$$

where s is the signal along the trajectory, N_i is the internal noise and N the variance of stimulus noise. If we assume that the distribution of dots of the stimuli

follow a Poisson distribution (as there are 16 384 positions for the 360 dots), then signal strength (given by the mean dot number) should increase directly with stimulus area, and the noise (given by the square-root of the variance) should increase with the square-root of stimulus area. Thus, when N_i is small compared with the stimulus noise, d' should increase with the square-root of stimulus area (with slope of 0.5 on log-log co-ordinates), when the non-signal sectors were blank. When the non-signal sectors were filled noise, N remains constant with stimulus area, so d' should increase linearly with stimulus area (unit slope on log-log co-ordinates). These two predictions are indicated by the dotted and dashed lines of Fig. 3.

Inspection shows that the data tend to follow these predictions. The curves for the three different types of motion have very similar slope, and are virtually superimposed, straddling the theoretical curves. Table 1 reports the summation indexes for each observer (defined as the slopes of the curves on log-log co-ordinates), together with their associated S.E. Most of the indexes were within a S.E. of the predictions.

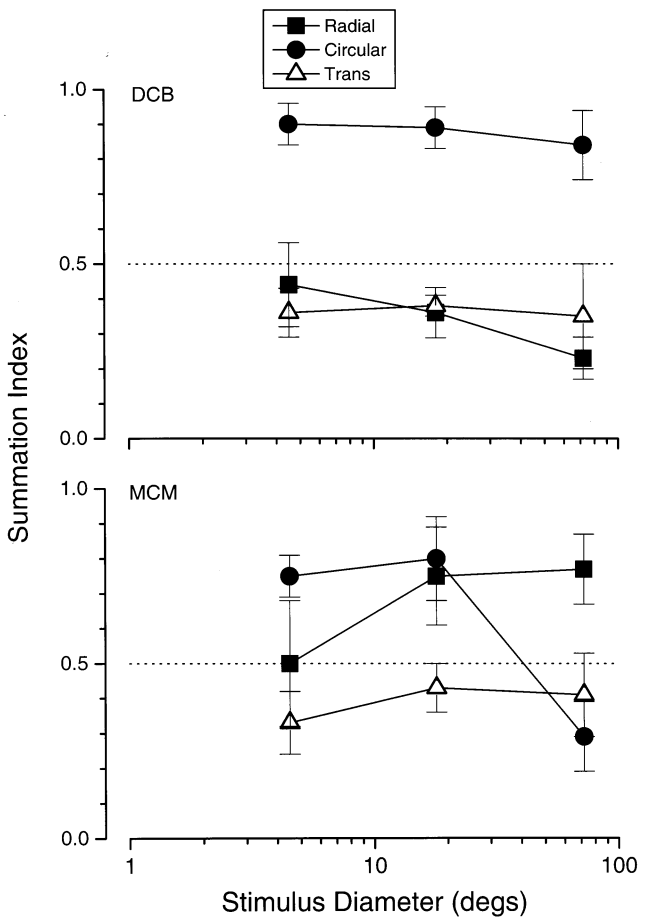

Fig. 8. Summation indexes for the data of Fig. 7, with error bars showing ±1 S.E., as a function of image size (outer diameter of annulus). The dashed line show predictions of the ideal integrator (0.5).

It should be stressed that as this stimulus is divided into multiple sectors positioned at maximum distance from each other, integration of radial and circular motion across these sectors could not be achieved by translation detectors. The motion of the different sectors was always in different directions, particularly where there were few sectors: for only two sectors, the local motion within each sector is in opposite directions, and for four sectors the motion is orthogonal. This type of stimulus, or an adaptation of it, was therefore used for most of the experiments of this study.

Before investigating receptive field size, we measured summation with other curtailment regimes, to look for possible inhomogeneities in summation. We also used a subject who was completely naïve to the goals of the experiment, to eliminate possible biases. As before, the full stimulus had 10° diameter, but could be curtailed in one of three different ways: by decreasing circle diameter (from 2.5 to 10°); by systematically reducing the circle to a narrow sector (varying from 22.5 to 360 clock°); and by reducing the stimulus to a discrete number (1–16) of sectors, each subtending 22.5 clock°, positioned so as to be maximally distant (as for Fig. 3). Fig. 4 shows the results for radial, circular and translational motion for three different methods of stimulus curtailment. For all three types of stimulus curtailment, sensitivity for radial, circular and translational motion improved steadily with image size at about the same rate (see Table 1 for summation indexes). This agrees well with the results of the previous study for 'windmill' curtailment, reproduced in Fig. 3. They also imply that summation for motion sensitivity does not depend on the shape of the stimulus, but only on the total area. It also shows that summation occurs at least up to 10°, the diameter of the largest circle.

An important result of the previous study is that the presence of noise outside the signal sectors decreases sensitivity (Fig. 3(C and D)), suggesting that the noise of the non-signal sectors is compulsorily integrated by the complex-motion unit. We examined this more directly by investigating the effect of adding noise sectors to the stimulus: four signal sectors were always displayed, but the number of noise sectors varied from 0 to 12. Fig. 5 plots the results as a function of total stimulus area: 25% refers to zero noise sectors and 100% to 12 noise sectors. Sensitivity decreased steadily as more noise sectors were added, irrespective of whether the noise abutted the signal sectors, or was in isolation. The summation indexes (shown in Table 1) are near −0.5, again consistent with an ideal integrator. Here signal strength is constant, and total noise varies with the square-root of stimulus area, so signal-to-noise ratios should decease with the square-root of signal area (dashed lines). This result reinforces previous evidence that complex motion is mediated by detec-

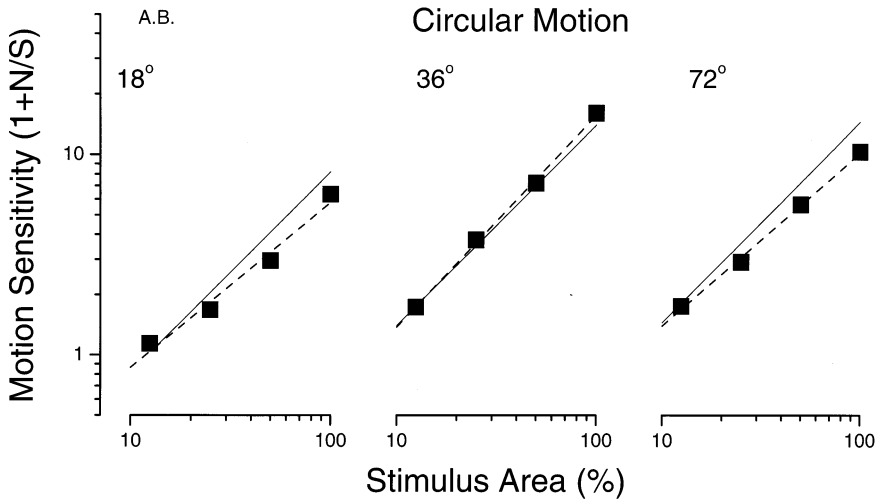

Fig. 9. Motion sensitivity of circular motion of an annulus curtailed into multiple sectors curtailment, for three different annuli sizes, when the non- signal sectors are filled with incoherent noise. A.B. was naïve to the aims of the experiment. The dotted line represents a linear relationship between sensitivity and image sizing, corresponding to the theoretical predictions of an ideal integrator. The summation indexes for the three image sizes were 0.82 ($\pm$0.08), 1.05 ($\pm$0.03) and 0.86 ($\pm$0.03), all with correlation coefficients greater than 0.99.

tors that summate all motion energy falling within their extensive receptive field.

3.2. Receptive field size

The main goal of the current study was to probe the limits of integration, to obtain an estimate of the size of the receptive fields of the mechanisms. At first, one may suggest that the simplest technique would be to increase the size of a stimulus (like the experiment of Fig. 4(A)), until sensitivity became constant. However, this technique is susceptible to potential difficulties arising from retinal inhomegeneity for motion sensitivity, and possible differences in preferred speed with eccentricity. Thus summation curves could deviate from the theoretical expectations, not because the limits of summation have been reached, but because increasing stimulus size causes it to stimulate more eccentric regions where velocity may not be ideal.

We therefore chose annular stimuli, designed to stimulate a region of peripheral visual field, where sensitivity should be reasonably homogeneous, avoiding the complications of inhomogeneities of central vision. An example of an annular stimulus curtailed to four sectors is illustrated in Fig. 1(D). The inner diameter was 14 cm and the outer 20 cm. Image size was varied by varying viewing distance, with the effect of not only changing overall size, but also scaling element size and speed proportionally.

To investigate the effects of image speed, and to establish the best velocity for these eccentric stimuli, we first measured motion sensitivity at various speeds for annular stimuli of various sizes (varied by varying viewing from 14 to 220 cm, varying the outer diameter from 4.5 to 72°). Speed was varied by varying the inter-frame interval between displacements, from 5.5 to 176 ms. Fig. 6 shows the dependency of motion sensitivity on image speed, for the three types of complex motion. The curves show a clear inter-relationship between eccentricity and velocity, with the more eccentric stimuli being more sensitive at higher velocities. For each stimulus size, the penultimate velocity (inter-frame interval of two video frames—11 ms), provided near maximal sensitivity and was therefore used for all subsequent experiments in this section. However, we should note that because the procedure varied not only eccentricity, but also dot displacement and dot size (hence average spatial frequency), it cannot be certain that the crucial factor was eccentricity per se, or displacement or spatial frequency (cf. [35]).

We then studied the effect of curtailment of these large annuli Fig. 7. The curtailment was like that for Fig. 4(C), except that the initial stimuli were annuli rather than circles, curtailed into sectors of 22.5 clock°, positioned to be maximally distant from each other. As before, the predicted performance of the ideal integrator is a square-root relationship, illustrated by the dashed lines. Although there was some variation between subjects, summation was observed for most conditions, at least up to 18°. For MCM the summation was strong even for 72° stimuli.

Fig. 8 plots the summation indexes (slope of the best linear regression of log sensitivity against log area), together with its associated error. For MCM the summation indexes were high for both radial and circular motion at most diameters. For DCB, there was far stronger summation for circular motion, far greater than 0.5, the theoretical expectation for an ideal integrator. For the other types of motion, summation still occurred, but slightly less than the predicted slope of 0.5.

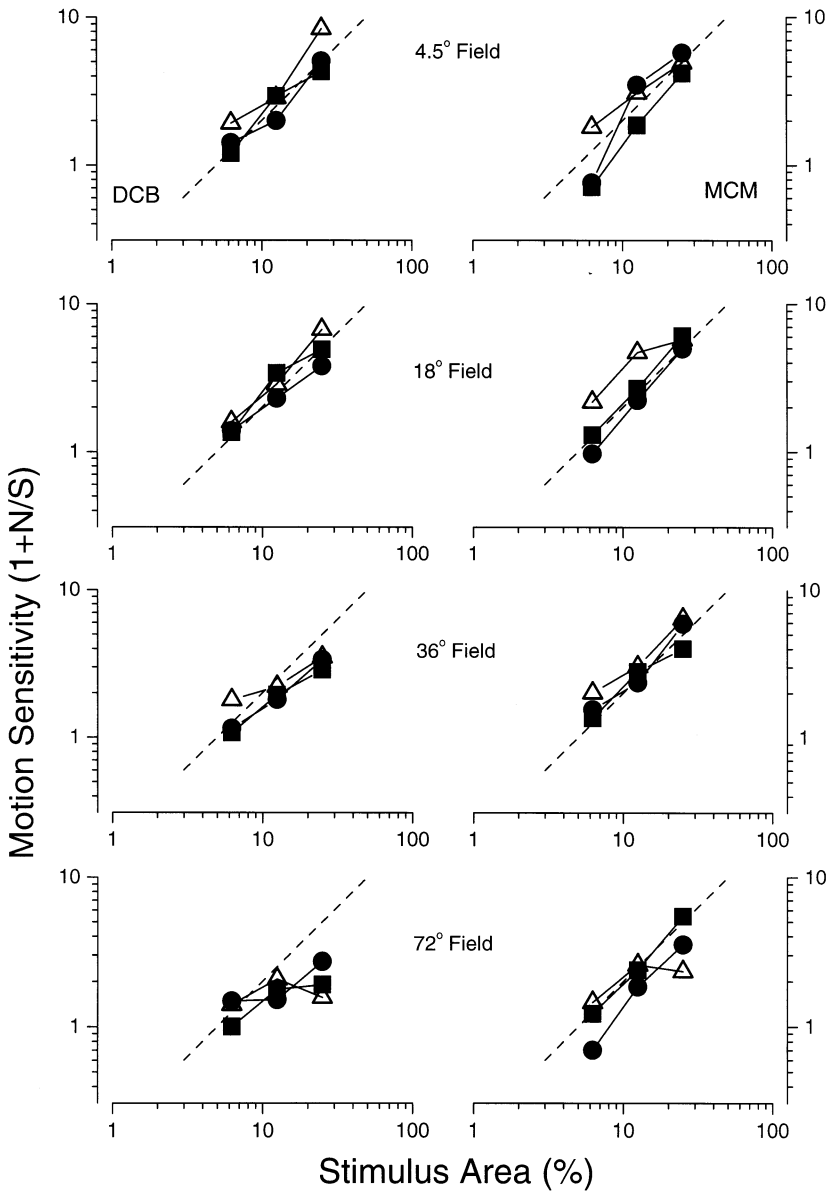

Fig. 10. Motion sensitivity radial, circular and translational motion of a curtailed annulus. The stimulus contained four opposing sectors, in which one, two or four were filled with coherent motion and the others with incoherent noise. The position of the signal sectors was randomised between trials. The dotted line represents a linear relationship between sensitivity and image size, corresponding to the theoretical predictions of an ideal integrator.

To accentuate the effects of summation, we repeated the experiment with the non-signal sectors filled with uncorrelated noise, as for the experiments of (Fig. 3(C and D)). Here the ideal integrator predicts a linear relationship between sensitivity and stimulus area under these conditions, illustrated by the dashed lines of Fig. 9. The results for a single naïve observer follow the predictions well for all image sizes.

With all the non-signal sectors filled with noise, sensitivity was greatly reduced, so much so that the task was impossible with only one signal sector, and difficult with only two sectors. Thus the curves of Fig. 9 lack the crucial points that should show summation up to four sectors, where the local motion between sectors is either opposite or orthogonal for radial and circular motion. We therefore repeated the experiment, using only four sectors positioned along the horizontal and vertical axes (as illustrated in Fig. 1(D)), given that the results of Fig. 5 show that masking is equally effective for non-abutting stimuli. Again sensitivity was measured as a function of stimulus area, while the non-signal sectors were filled with incoherent noise. Fig. 10 shows the results for the three types of motion, for three sizes of stimulus (again changing stimulus size by changing viewing distance). For the 4.5, 18 and 36° stimuli, sensitivity for both observers increased linearly with

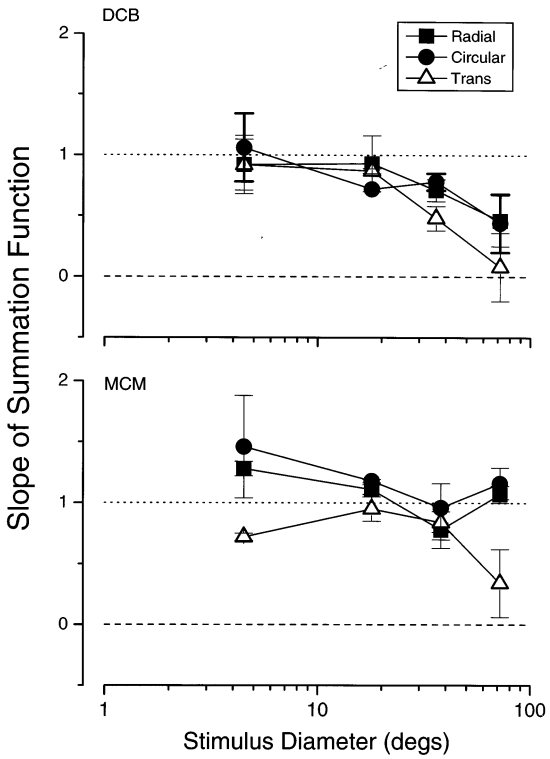

Fig. 11. Summation indexes for the data of Fig. 10, with error bars showing ±1 S.E., as a function of image size (outer diameter of annulus). The dashed line at slope one indicates the performance an ideal integrator.

stimulus size, for all motion types. However, for the largest stimulus size, the dependence on stimulus size was less than linear, particularly for DCB. This implies that summation was not perfect at this image size.

Fig. 11 plots the summation indexes for the two subjects. For DCB, the index remains near one for outer diameters up to 18°, then begins for all three types of motion. With MCM the pattern was different, with slopes of one or greater for radial and circular motion at all stimulus sizes, but translational motion shows incomplete summation at 72°.

4. Discussion

The experiments reported here provide further evidence for spatial integration of optic flow fields within the visual system. Sensitivity varied with the area of the stimulus, for three different types of images curtailment. The increase closely followed the theoretical prediction in all cases, suggesting the existence of mechanisms that integrate information over large regions of space, even when the sectors carrying motion information are non abutting. When extra segments of incoherent noise were introduced, sensitivity was reduced predictably, with the inverse of the square-root of the area. This showed that the summation was obligatory, and sensitivity could be either increased or decreased by adding extra signal or noise. The sensitivity to optic flow motion was very broadly tuned for speed, over a wide range, consistent with the physiology of MST neurones [12,36].

The experiments with annuli showed spatial summation over very large extents, consistent with integration being performed by neurones with large receptive fields. The exact size of the neurones is difficult to assess accurately, and shows variations from one observer to another. However, strong summation occurred for image sizes of at least 36° and up to 72° for MCM. Larger stimuli could not be practically generated on a flat screen. The existence of large receptive fields for optic flow analysis is consistent with the electrophysiological evidence showing large receptive fields ranging from 10 to 100°, often extending over both hemifields [9,10,12,14].

In humans, summation has been demonstrated previously with different techniques. Anderson and Burr

Table 1
Summation index for the observers for various conditions

Observer	Prediction	Radial	Circular	Translation
DB (Fig. 3(A): no-noise)	0.5	0.50 ± 0.06	0.54 ± 0.03	0.47 ± 0.05
MCM (Fig. 3(B): no-noise)	0.5	0.54 ± 0.08	0.66 ± 0.05	0.45 ± 0.08
CQ (Fig. 4: circles)	0.5	0.57 ± 0.09	0.58 ± 0.13	0.51 ± 0.13
CQ (Fig. 4: sectors)	0.5	0.68 ± 0.08	0.61 ± 0.14	0.79 ± 0.03
CQ (Fig. 4: windmills)	0.5	0.40 ± 0.03	0.49 ± 0.10	0.38 ± 0.10
DB (Fig. 3(C): with-noise)	1.0	1.07 ± 0.11	0.91 ± 0.11	1.12 ± 0.07
MCM (Fig. 3(D): with-noise)	1.0	0.89 ± 0.13	0.95 ± 0.06	0.91 ± 0.06
DB (Fig. 5: masking)	−0.5	−0.71 ± 0.04	−0.30 ± 0.03	
MCM (Fig. 5: masking)	−0.5	−0.60 ± 0.02	−0.60 ± 0.05	
Normalised average	0.5	0.55 ± 0.03	0.52 ± 0.04	0.52 ± 0.05

The index was defined as the best linear fit of log sensitivity against log area, together with the S.E. of the fit. This is equivalent to calculating the index i of the power function $S \propto A^i$, where S is sensitivity and A is area. In all cases the correlation coefficient was greater than 0.9, with an average of 0.97. The normalised average is the average of the indexes in a given column, normalised so the prediction is 0.5. The errors are the S.E. of the mean, without taking individual errors into account.

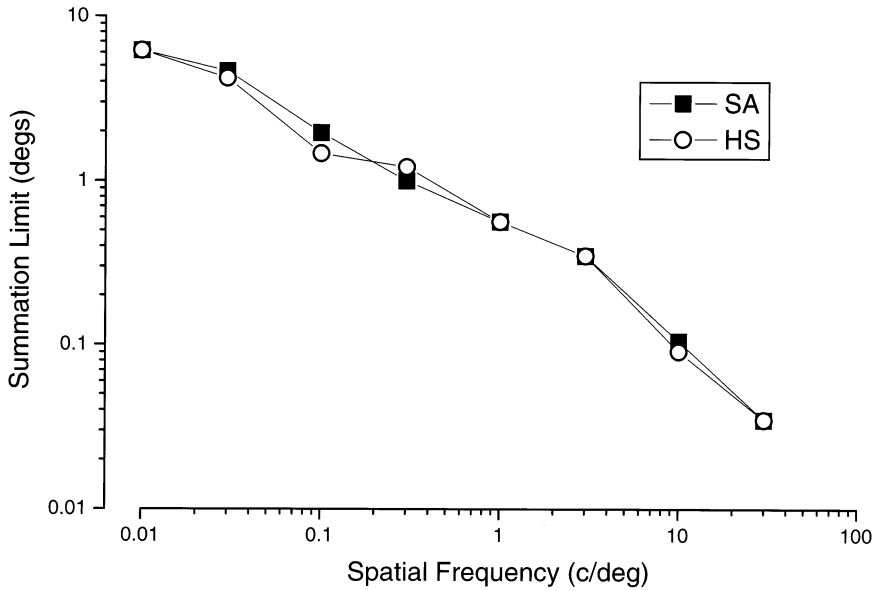

Fig. 12. Estimates of the extent of spatial summation for contrast sensitivity for translational motion (reproduced with permission from Fig. 4 of Anderson and Burr [1]).

[1,37] showed that the extent of summation for contrast sensitivity of gratings varied with the spatial frequency of the grating. Fig. 12 summarises the main result of the study: high frequency gratings (above 20 cd) summed up to only 2′ of arc, while low-frequency gratings summed over much larger regions, 8° at 0.01 cd. Receptive field size did not scale linearly with preferred spatial frequency, but with an approximate square-root relationship.

The stimuli of the present study were broadband, and therefore difficult to compare directly with Anderson and Burr's results. Fig. 13 shows an example of the amplitude spectrum of the stimulus, expressed in cycles/picture. The upper ordinate shows the spectrum in cycles/degree (cd) at the closest viewing distance. There is a considerable spread of spatial frequencies, but not so great as to excite equally all motion detectors. The triangular symbols show the response strength of various motion detectors of different spatial-frequency tuning, using sensitivity and bandwidth estimates of Anderson and Burr [38]. These simulations suggest that the most sensitive mechanisms for these stimuli are those tuned to about 0.2 cd, predicting summation over 1° of visual angle (from Fig. 12). Yet the extent of spatial summation observed here was 30–70°, one and a half orders of magnitude greater.

We suggest that the reason for the difference in the summation estimates reflects different extents of summation at different stages of motion analysis, and the two different techniques probe different stages. The previous study [2] showed that there is very little summation for contrast sensitivity of complex stimuli. We suggested, with strong supporting evidence, that contrast sensitivity may be limited by early stages of motion analysis, probably V1 (where neurones have a clear contrast threshold), while the signal to noise technique may probe higher levels, such as MST. Thus the dependence of receptive field size on spatial frequency probably reflects the properties of neurones in an early stage of motion analysis (possibly V1), rather than the higher level neurones responsible for optic flow field analysis. An interesting prediction, that could be tested specifically in future studies, is that the spatial extent of these receptive fields for optic flow (measured by signal-to-noise techniques) may be largely independent of the spatial frequency content of the stimuli. Some evidence along these lines has been provided for translational motion [39].

This study did not probe specifically the shape of the receptive fields, as previous studies have with grating stimuli (reporting putative receptive fields with unit aspect ratio: [1,37]. Here the studies probing the limits of integration used symmetric curtailment, so there was little information of receptive field size. There was sometimes a tendency for radial motion to show more summation than the other types of motion, but this effect was not consistent over observers or conditions. The average summation indexes for the smaller (10°) stimuli (normalised and averaged over subjects and conditions in Table 1) were very similar for the three types of complex motion. The degree of summation tended to be independent of the shape of the stimuli, and of whether they were confined to separate sectors or formed a single sector or disk Fig. 4. The stimuli of this study contained only a single component of motion (either radial, rotation or translational) falling along the 'cardinal axes' of optic flow space. However, this does not imply that all visual neurones are tuned in

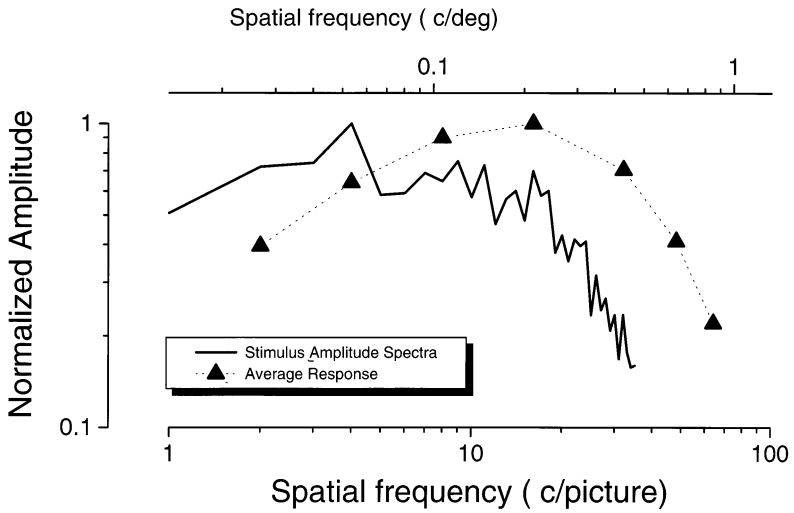

Fig. 13. Typical spatial amplitude spectrum of the stimuli used in this experiment (continuous curve). The triangular symbols show the predicted response of the spatially selective mechanisms revealed by masking studies [38].

these directions; there could well exist neurones selective to intermediate directions of motion, such as spiral motion, as the recent physiological and psychophysical studies suggest (e.g. [13,14,31]).

The properties of the motion detectors revealed by this study, large receptive fields, integration of information over disparate regions, and relative insensitivity to speed make them ideal for computing complex tasks such as optic flow analysis and heading (see [40]).

Acknowledgements

Supported by Italian CNR and MURST, and NIH grants 2R01-EY7861-06 and NSF grant SBR-930126.

References

[1] Anderson SJ, Burr DC. Receptive field size of human motion detection units. Vis Res 1987;27:621–35.
[2] Morrone MC, Burr DC, Vaina LM. Two stages of visual processing for radial and circular motion. Nature 1995;376:507–9.
[3] Gibson JJ. The Ecological Approach to Visual Perception. Boston: Houghton Mifflin, 1979.
[4] Koenderink JJ, van Doorn AJ. Invariant properties of the motion parallax field due to the movement of rigid bodies relative to the observer. Opt Acta 1975;22:773–91.
[5] Koenderink JJ, van Doorn AJ. Local structure of movement parallax of the plane. J Opt Soc Am 1976;66:717–23.
[6] Koenderink JJ. Optic flow. Vis Res 1986;26:161–79.
[7] Verri A, Girosi F, Torre V. Differential techniques for optical flow. J Opt Soc Am 1990;7:912–22.
[8] Saito HA, Yukie M, Tanaka K, Hikosaka K, Fukada Y, Iwai E. Integration of direction signals of image motion in the superior temporal sulcus of the macaque monkey. J Neurosci 1986;6:145–57.
[9] Sakata H, Shibutani H, Ito Y, Tsurugai K. Parietal cortical neurons responding to rotary movement of visual stimulus in space. Exp Brain Res 1986;61:658–63.
[10] Tanaka K, Hikosaka K, Saito H, Yukie M, Fukada Y, Iwai E. Analysis of local and wide-field movements in the superior temporal visual areas of the macaque monkey. J Neurosci 1986;6:134–44.
[11] Tanaka K, Fukada Y, Saito H. Underlying mechanisms of the response specificity of expansion/contraction and rotation cells in the dorsal part of the medial superior temporal area of the macaque monkey. J Neurophysiol 1989;62:642–56.
[12] Tanaka K, Saito H. Analysis of motion of the visual field by direction, expansion/contraction, and rotation cells clustered in the dorsal part of the medial superior temporal area of the macaque monkey. J Neurophysiol 1989;62:626–41.
[13] Graziano MSA, Andersen RA, Snowden RJ. Tuning of MST neurons to spiral stimulus. J Neurosci 1994;14:54–67.
[14] Duffy CJ, Wurtz RH. Sensitivity of MST neurons to optic flow stimuli. I. A continuum of response selectivity to large-field stimuli. J Neurophysiol 1991;65:1329–45.
[15] Duffy CJ, Wurtz RH. Sensitivity of MST neurons to optic flow stimuli. II. Mechanisms of response selectivity revealed by small field stimuli. J Neurophysiol 1991;65:1346–59.
[16] Duffy CJ, Wurtz RH. Response of monkey MST neurons to optic flow stimuli with shifted centers of motion. J Neurosci 1995;15:5192–208.
[17] Orban GA, Lagae L, Verri A, Raiguel S, Xiao D, Maes H, Torre V. First-order analysis of optical flow in monkey brain. Proc Natl Acad Sci USA 1992;89:2595–9.
[18] Lagae L, Maes H, Raiguel S, Xiao DK, Orban GA. Responses of the macaque STS neurons to optic flow components: a comparison of areas MT and MST. J Neurophysiol 1994;71:1597–626.
[19] Lappe M, Bremmer F, Pekel M, Thiele A, Hoffmann KP. Optic flow processing in monkey STS: a theoretical and experimental approach. J Neurosci 1996;16:6265–85.
[20] Duffy CJ, Wurtz RH. Optic flow, posture, and the dorsal visual pathway. In: Ono ET, McNaugton BL, et al., editors. Perception, Memory and Emotion: Frontiers in Neuroscience. Cambridge: Elsevier Science, 1997:63–77.
[21] Steinmetz MA, Motter BC, Duffy CJ, Mountcastle VB. Functional properties of parietal visual neurons: radial organization

of directionalities within the visual field. J Neurosci 1987;7:177–91.
[22] Andersen RA, Treue S, Graziano M, Snowden RJ, Quan N. From direction of motion to pattern of motion: hierarchies of motion analysis in the visual cortex. In: Ono T, Squire LR, Raichle ME, Perrett D, Fukuda M, editors. Brain Mechanisms Of Perception And Memory. New York: Oxford University Press, 1993.
[23] Maunsell JH, Essen DCV. Functional properties of neurons in middle temporal visual area of the macaque monkey. I. Selectivity for stimulus direction, speed, and orientation. J Neurophysiol 1983;49:1127–47.
[24] Ungerleider LG, Desimone R. Cortical projections of visual area MT in the macaque. J Cogn Neurosci 1986;248:147–63.
[25] Regan D, Beverley KI. Looming detectors in the human visual pathway. Vis Res 1978;18:415–21.
[26] Regan D, Beverley KI. Motion sensitivity measure by a psychophysical linearizing technique. J Opt Soc Am 1981;71:958–9.
[27] Regan D, Beverley KI. Visual responses to vorticity and the neural analysis of optic flow. J Opt Soc Am 1985;A2:280–3.
[28] Beverley KI, Regan DM. Visual perception of changing size: the effect of object size. Vis Res 1979;19:1093–104.
[29] Lappin JS, Norman JF, Mowafy L. The detectability of geometric structure in rapidly changing optical patterns. Perception 1991;20:513–28.
[30] Freeman TC, Harris MG. Human sensitivity to expanding and rotating motion: effects of complementary masking and directional structure. Vis Res 1992;32:81–7.
[31] Snowden RJ, Milne AB. The effects of adapting to complex motions: position invariance and tuning to spiral motions. J Cogn Neurosci 1996;8:412–29.
[32] Te Pas SF, Kappers AML, Koenderink JJ. Detection of first-order structure in optic flow fields. Vis Res 1996;36:259–70.
[33] Bex PJ, Makous W. Radial motion looks faster. Vis Res 1997;37:3399–3405.
[34] Watson AB, Pelli DG. QUEST: a Bayesian adaptive psychometric method. Percept Psychophys 1983;33:113–20.
[35] Burr DC, Ross J. Contrast sensitivity at high velocities. Vis Res 1982;22:479–84.
[36] Orban GA, Lagae L, Raiguel S, Xiao D, Maes H. The speed tuning of middle superior temporal (MST) cell responses to optic flow components. Perception 1995;24:269–85.
[37] Anderson SJ, Burr DC. Spatial summation properties of directionally selective mechanisms in human vision. J Opt Soc Am 1991;A8:1330–9.
[38] Anderson SJ, Burr DC. Receptive field properties of human motion detector units inferred from spatial frequency masking. Vis Res 1989;29:1343–58.
[39] Yang Y, Blake R. Broad tuning for spatial frequency of neural mechanisms underlying visual perception of coherent motion. Nature 1994;371:793–6.
[40] Bradley DC, Maxwell M, Andersen RA, Banks MS, Shenoy KV. Mechanisms of heading perception in primate visual cortex. Science 1996;273:1544–7.